Sliding Mode Controller Applied to Coupled Inductor Dual Boost Inverter

Yu Fang[†], Songyin Cao[*], and Pat Wheeler[**]

[†*] College of Information Engineering, Yangzhou University, Yangzhou, China
[**]Department of Electrical and Electronic Engineering, The University of Nottingham, Nottingham, UK.

Abstract

A coupled inductor-dual boost-inverter (CIDBI) with differential structure has been presented to be applied to micro-inverter photovoltaic module system because of its turn ratio of high-voltage level. However, it is hard for CIDBI converter with conventional PI regulator to be designed stable and achieve good dynamic performance, given the fact that it is a high order system. In view of this situation, a sliding mode control (SMC) strategy is introduced in this paper, and two different sliding mode controllers (SMCs) are proposed and adopted in the left and right side of the two Boost sub-circuits respectively to implement corresponding regulation of voltage and current. The schemes of the SMCs have been elaborated in this paper including the establishment of the system variable structure model, the selection of the sliding surface, the determination of the control law, and the presentation of the reaching conditions and sliding domain. Finally, the mathematic analysis and the proposed SMC are verified by the experimental results.

Key words: Coupled inductor, Micro inverter, Photovoltaic (PV) power generation, Sliding mode control

I. INTRODUCTION

Grid-connected micro-inverter is an effective way to solve the hot spot effect of photovoltaic modules and improve the efficiency of photovoltaic power generation. There are two main grid-connected power generation methods for low-voltage photovoltaic modules. 1) Single-stage inverters are connected to the grid by line transformer boost mode. 2) Two-stage inverter consist of front-stage DC-DC boost circuit and back-stage inverter. In the first method, when the voltage of photovoltaic module is low, the turn ratio of line transformer is large, and hence the power loss of transformer is large. In the second method, two-stage circuit is adopted, and the conversion efficiency of the system is not high. It can be seen that these two methods are not conducive to the efficient generation of small and medium power photovoltaic cells to the grid.

The CIDBI that proposed in work [1] can meet the requirements of voltage boost of photovoltaic modules and AC grid-connected, that is, to realize one-stage transformerless grid-connected.

The differential CIDBI, as shown in Fig.1 presented in work [1], is composed of the two coupled inductor boost circuits that generates an ac output voltage larger than dc input, depending on the instantaneous duty cycle and turn ratio of the coupled inductor as well, and uses only one power processing stage. Fig.1 shows that there is one DC source B_1, L_1 and L_2 commonly share the same magnetic core, while L_3 and L_4 use another, so the two coupled inductors are constructed. One boost circuit consists of L_1, L_2, C_2, switches T_1, T_2 and their body diodes D_1, D_2, the other boost circuit consists of L_3, L_4, C_3, switches T_3, T_4 and their body diodes D_3, D_4. It is clear that the right-side circuit and the left one represent boost converters with coupled inductor. The work [1] tells us that CIDBI can be employed as micro inverter integrated with much lower voltage PV array and even achieve high energy conversion

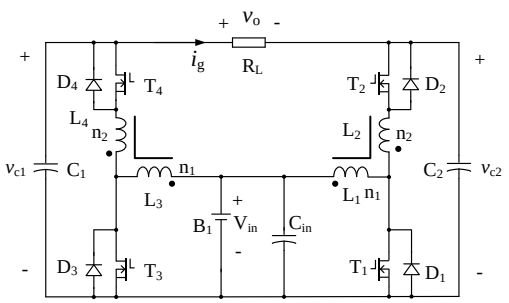

Fig. 1. Main circuit of CIDBI.

Manuscript received Month. Date, Year; accepted June, 27, 2019
Recommended for publication by Associate Editor Gil-Dong Hong.
[†]Corresponding Author: yfang@yzu.edu.cn
Tel: +86-514-87978319, Fax: +86-514-87971865, Yangzhou University
[*]College of Information Engineering, Yangzhou University, Yangzhou, China.
[**]Department of Electrical and Electronic Engineering, The University of Nottingham, Nottingham, UK.

efficiency because of its one-stage boost circuit architecture. However, It is difficult to achieve the tradeoff between stability and fast dynamic response of CIDBI by using traditional linear controllers, which brings energy loss to sudden changes in photovoltaic applications.

In order to obtain a smoother grid current i_g, we add an AC output inductor L_{ac} on the basis of Fig.1, as shown in Fig.2. in which the current i_g through L_{ac} will be shaped by adapting the voltage difference (v_{c1}-v_{c2}). In this paper, two different sliding mode controllers are proposed and adopted in the left and right side circuit of the CIDB respectively to realize grid-connected power generation, and the SMCs for grid-connected power generation are discussed and analyzed, so that the energy of low-voltage photovoltaic modules can be transferred into power grid by CIDBI with good performance.

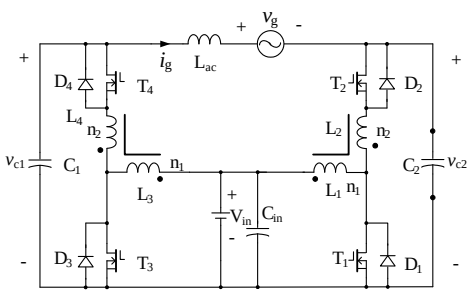

Fig.2. Main circuit of the CIDBI after insertion of L_{ac}.

sliding modes, as shown in Fig.3. In order to generate an ac output current i_g from dc sources, the left-side circuit will be controlled to shape the grid current ig, and the right-side one to make the output voltage stable which is close to v_{C2}* (reference voltage). These two parts of controller can realize decoupling control. Next, the error state equation of the left and right circuit will be deduced.

A. Right-Side Circuit

CIDBI is based on the boost converter, hence the voltage v_{C2} must never fall below V_{in}. That is to say the output voltage is a dc-biased sinusoidal voltage as presented in equation(1) and the equation (1) defines the reference for v_{C2}.

$$v_{c2}^{*}(t) = V_m^{*}\sin(\omega t + \pi) + V_{dc}^{*} \tag{1}$$

Assuming that the grid voltage is as follows：

$$v_g(t) = V_g \sin(\omega t) \tag{2}$$

When in steady operation, the grid current should follow the reference current i_g^{*}. Here assuming the reference grid current and grid current are as follows:

$$i_g^{*}(t) = I_g^{*}\sin(\omega t) \tag{3}$$

$$i_g(t) = I_g \sin(\omega t) \tag{4}$$

Due to that the differential output is constructed by the left-side and right-side circuits, the reference ac voltage component is given as follows:

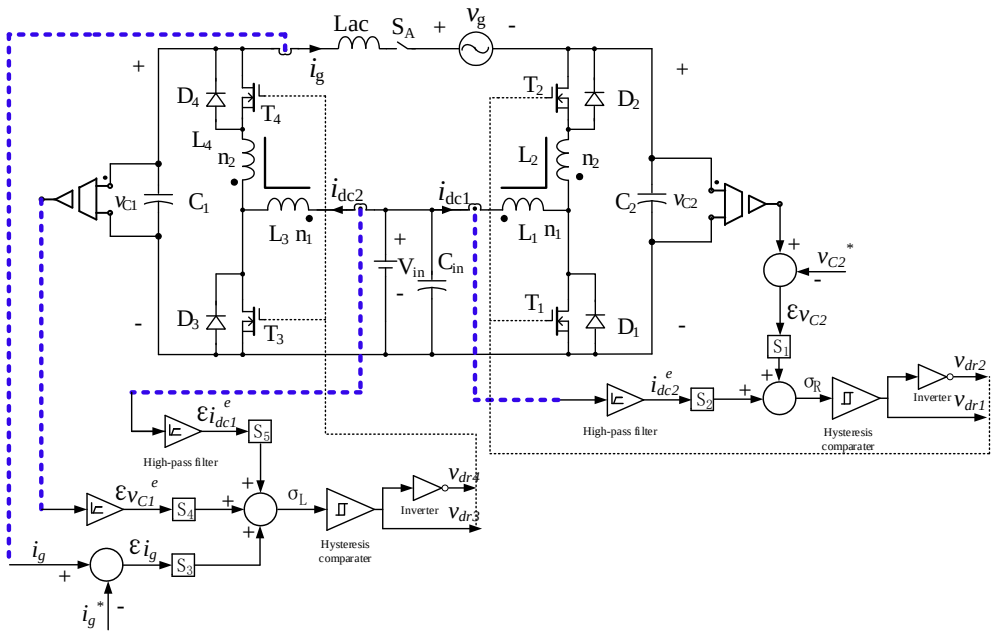

Fig.3. The schematic diagram for CIDBI with two sliding mode controllers.

II. ANALYSIS AND DESIGN OF SMCS

The main circuit diagram of CDBI shown in the Fig.2 can be divided into two subsystems that are controlled by different

$$V_m^{*} = V_g / 2 \tag{5}$$

In order to keep the voltage v_{c2} higher thanV_{in} all the time, the following inequality is met.

$$V_{dc}^{*} > V_{dc} + V_g / 2 \tag{6}$$

v_{C2}^*can be achieved by controlling T_1 and T_2 in the right-side boost circuit, and the pulse control signals v_{dr1} and v_{dr2} should be complementary. In light of switching states, the right side of the converter can be equivalent to two sub-circuits as shown in the Fig.4. And the left side of the CIDBI can be considered as the current source. So the calculation formula of duty cycle ratio $d_R(t)$ for the right side is as follows.

$$d_R(t)=\frac{v_{c2}^*(t)-V_{in}}{v_{c2}^*(t)+N\cdot V_{in}}=\frac{V_m^*\sin(\omega t+\pi)+V_{dc}^*-V_{in}}{V_m^*\sin(\omega t+\pi)+V_{dc}^*+N\cdot V_{in}} \quad (7)$$

Where, N is the turn ratio of the coupled inductor (seen in the Fig.1: n_2/n_1).

The average power of the output should be equal to that of the input according to the instantaneous power theory. So the equation (8) can be gotten.

$$V_{in}\cdot i_{dc1}^*(t)=C_2\cdot v_{c2}^*(t)\cdot\frac{d(v_{c2}^*(t))}{dt}-v_{c2}^*(t)i_g^*(t) \quad (8)$$

Substituting the expression (1), (2), (4) and (5) into the equation (8), the reference value i_{dc1}* for dc input current can be expressed as (9).

$$i_{dc1}^*(t)=\frac{1}{V_{in}}\begin{bmatrix}\frac{1}{2}V_m^*\cdot I_g^*(1-\cos(2\omega t))-V_{dc}^*\cdot I_g^*\sin(\omega t)\\ -\omega C_2\cdot(V_{dc}^*\cdot V_m^*\cos(\omega t)-\frac{1}{2}(V_m^*)^2\sin(2\omega t))\end{bmatrix} \quad (9)$$

The expression (9) describes the average input current i_{dc1} through the coupled inductor L_1/L_2. In fact, the input current contains the high-frequency ripple current that can be neglected because this ripple current has no effect on the effective value of current.

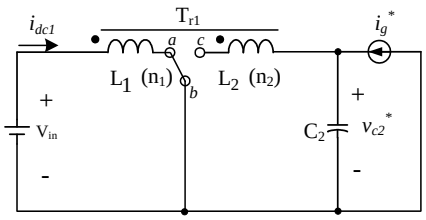

（a） T_1 is on and $T_2(D_2)$ off

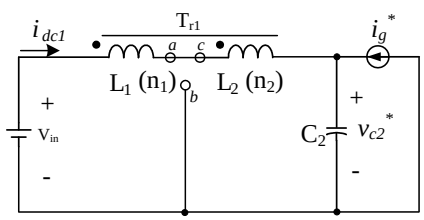

（b） $T_2(D_2)$ is on and T_1 off

Fig.4. The two structures of the right-side converter.

The switching function can be defined in the expression(10), where, $\gamma$is the state variable.

$$\gamma=\begin{cases}1 & \text{When } T_1 \text{ is ON and } T_2(D_2) \text{ off}\\ 0 & \text{When } T_1 \text{ is OFF and } T_2(D_2) \text{ on}\end{cases} \quad (10)$$

It is clear that the corresponding output energy will increase when γ=1 happens. In this state, the inductor L_1 and the output capacitance C_2 are decoupled and the current through L_1 is increased linearly, i.e, the energy storage; i_g flows to C_2 as shown in the Fig. 4(a). When γ=0 occurs, the energy will be transferred to C_2 by the coupled inductor L_1/L_2 as shown in the Fig.4(b).

It can be seen from the Fig.4 that there are two error variables that are defined εv_{C2} for output capacitance voltage and εi_{dc1} for coupled inductor current respectively in the expression (11).

$$\begin{cases}\varepsilon v_{C2}=v_{C2}-v_{C2}^*\\ \varepsilon i_{dc1}=i_{dc1}-i_{dc1}^*\end{cases} \quad (11)$$

As a consequence, the state error equation of the right-side converter can be written as (12).

$$\dot{x}=\mathrm{A}x+\mathrm{B}\gamma+\mathrm{D} \quad (12)$$

Where,

$$x=[\varepsilon v_{C2},\ \varepsilon i_{dc1}]^{\mathrm{T}} \quad (13)$$

$$\mathrm{A}=\begin{bmatrix}0 & \frac{1}{C_2}\\ -\frac{1}{L_1\cdot(1+N)} & 0\end{bmatrix} \quad (14)$$

$$\mathrm{B}=\begin{bmatrix}-\frac{i_{dc1}}{C_2}\\ \frac{v_{c2}+N\cdot V_{in}}{L_1\cdot(1+N)}\end{bmatrix} \quad (15)$$

$$\mathrm{D}=\begin{bmatrix}\frac{i_g^*+i_{dc1}^*}{C_2}\\ \frac{V_{in}-v_{c2}^*}{L_1\cdot(1+N)}\end{bmatrix} \quad (16)$$

It is noted that the low-frequency reference functions, when compared to the switching frequency, can be considered as quasistatic, in such a way that the term of derived function for the reference is, in general, neglected in the equation (12).

B. Left-Side Circuit

The left-side subsystem is looked as the current source and controlled to shape the grid current. Actually, the voltage of the L_{ac} can be regulated only if the voltage v_{C1} across the C_1 is controlled, as the result that the grid current i_g is gotten. Additionally, since the inductor L_{ac} is designed to filer the high-frequency switching ripple, its steady-state low-frequency voltage is small, and also the voltage v_{C1} should be close to (v_{C2}+v_g). So v_{C1} can be expressed as (17).

$$v_{C1}^*(t)\approx V_m^*\sin(\omega t)+V_{dc}^* \quad (17)$$

The ac component of the expression (17) is complementary to that of the expression (1), so the phase difference is 180°, besides the equations of duty cycle ratio $d_L(t)$ and i_{dc2}^* are similar to (7) and (9), respectively, with π rad added to the arguments of sine or cosine function (or simply the terms in sin(ωt) and cos(ωt) change their signs, while the terms

involving 2ωt remain unchanged).

In order to follow i_g^*, the switches T_3 and T_4 in the left-side converter are controlled with some certain duty cycle ratio d_L, and their pulse control signals v_{dr3} and v_{dr4} should be complementary to each other. In light of the switching state, the left-side converter can be equivalent to two sub circuits as shown in the Fig.5, and the right-side converter is taken as voltage source in the Fig.5.

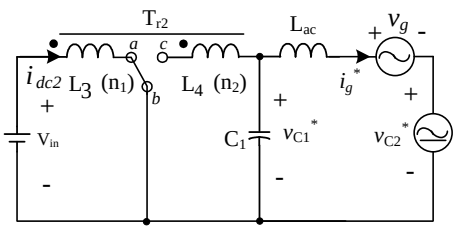

（a）T_3 is on and $T_4(D_4)$ off

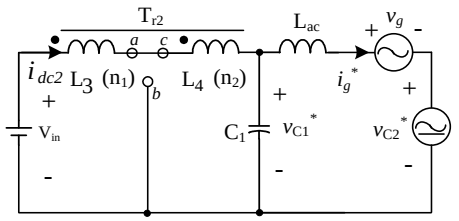

（b）$T_4(D_4)$ is on and T_3 off

Fig.5. The two structures of the left-side converter.

The two states in the Fig.5 can be described by the switching function as (18).

$$\lambda=\begin{cases}1 & \text{When } T_3 \text{ is on and } T_4(D_4) \text{ off}\\ 0 & \text{When } T_3 \text{ is off and } T_4(D_4) \text{ on}\end{cases} \tag{18}$$

Assuming that the error variable for filter L_{ac} is εi_g, the error variable for filter C_1 is εv_{C1}, and the error variable for coupled inductorL_3/L_4 is εi_{dc2}. As are shown in the expression (19).

$$\begin{cases}\varepsilon i_g=i_g-i_g^*\\ \varepsilon v_{C1}=v_{C1}-v_{C1}^*\\ \varepsilon i_{dc2}=i_{dc2}-i_{dc2}^*\end{cases} \tag{19}$$

After defining the error variables, the state error equation (20) can be written.

$$\dot{y}=\mathrm{A}'y+\mathrm{B}'\lambda+\mathrm{D}' \tag{20}$$

Where,

$$y=[\varepsilon i_g,\ \varepsilon v_{C1},\varepsilon i_{dc2}]^{\mathrm{T}} \tag{21}$$

$$\mathrm{A}'=\begin{bmatrix}0 & \frac{1}{L_{ac}} & 0\\ -\frac{1}{C_1} & 0 & \frac{1}{C_1}\\ 0 & -\frac{1}{L_3\cdot(1+N)} & 0\end{bmatrix} \tag{22}$$

$$\mathrm{B}'=\begin{bmatrix}0\\ -\frac{i_{dc2}}{C_1}\\ \frac{v_{C1}+N\cdot V_{in}}{L_3\cdot(1+N)}\end{bmatrix} \tag{23}$$

$$\mathrm{D}'=\begin{bmatrix}\frac{v_{C1}^*-v_{C2}^*-V_g}{L_{ac}}\\ \frac{i_{dc2}^*-i_g^*}{C_1}\\ \frac{V_{in}-v_{C1}^*}{L_3\cdot(1+N)}\end{bmatrix} \tag{24}$$

The derived function for the reference is neglected in the state error equation (20) as in the previous section. Through the above analysis, the error state equation of CIDBI is obtained.

III. CONTROL STRATEGY

The sliding mode takes place in the error state space, in which trajectory crossing the origin is designed. When the representative point of the system reaches the trajectory, it is confined close to it, and then directed toward the origin of the space(The origin represents the desired condition: null error) [10-16].This trajectory is called sliding surface (σ) which divides the space into two subspaces, with each one associated to a structure. One must ensure that the motion in the neighborhood of σ to be directed toward the surface, so that the representative point does not deviate from the specified trajectory [17-24]. This is known as the existence condition, mathematically expressed by (25).

$$\begin{cases}\dot{\sigma}<0, \text{When } \sigma>0\\ \dot{\sigma}>0, \text{When } \sigma<0\end{cases} \tag{25}$$

The practical sliding mode does not occur exactly on the sliding surface all the time, since this would require an infinite switching frequency. In fact, it happens very close to it, giving rise to what is called a quasi-sliding mode. It is a simple way to implement the quasi-sliding mode by hysteretic comparison between the actual state and the desired trajectory [25-27].

A. The Implementation of Right-Side SMC

The sliding mode surface σ_R is defined by the expression (26), which can be considered as the weight of error. If taking S_1 and S_2 is constant, the sliding mode surface is a straight line on the plane of $\mathcal{E}_{v_{C2}}\times\mathcal{E}_{i_{dc1}}$, and the slope is decided by $\alpha_R=S_1/S_2$. Among the expression (25), Units: S_2 is ohms; S_1 is dimensionless; and then α_R is Siemens.

$$\sigma_R=S_1\cdot\varepsilon_{v_{C2}}+S_2\cdot\varepsilon_{i_{dc1}} \tag{26}$$

Assuming that $S=[S_1,\ S_2]^{\mathrm{T}}$, the expression (25) can be expressed by (27).

$$\sigma_R=\mathrm{S}^{\mathrm{T}}x \tag{27}$$

Since the error variables are defined by(12), whenever the representative point lies below the switching line σ_R, the energy in the elements C_2 and L_1 is little, and thus γ is set to 1, conversely, the energy is surplus when the representative point lies above the switching line σ_R, and γ is set to 0. So the expression (28) can be gotten.

$$\gamma = \begin{cases} 1 & \text{When } \sigma_R < 0 \\ 0 & \text{When } \sigma_R > 0 \end{cases} \tag{28}$$

Due to that the error variables is very small and approaches to zero by comparison with the reference values, so the existing condition (25) for sliding mode surface on the right side can be written by (29) and (30).

$$\dot{\sigma}_R = S^T D < 0, \quad \sigma_R > 0 \tag{29}$$

$$\dot{\sigma}_R = S^T B + S^T D > 0, \quad \sigma_R < 0 \tag{30}$$

Substituting the matrix B and D into (29) and (30) respectively, the expression (31) and (32) can be gotten.

$$S_1 \cdot \frac{i_g^* + i_{dc1}^*}{C_2} + S_2 \cdot \frac{V_{in} - v_{C2}^*}{L_1 \cdot (1+N)} < 0 \tag{31}$$

$$S_1 \cdot \frac{i_g^* + i_{dc1}^* - i_{dc1}}{C_2} + S_2 \cdot \frac{v_{C2} - v_{C2}^* + (1+N) \cdot V_{in}}{L_1 \cdot (1+N)} > 0 \tag{32}$$

It can be concluded from (31) and (32) that the condition is S_1 and S_2 choose non-negative values if there is existence of the sliding mode surface as presented in (26).

If the actual system adopts the fixed hysteresis width 2δ in the Fig.6, the control rules can be rewritten into (33). And the phase plane trajectory will oscillate on both sides of the sliding mode surface (σ_R=0), as shown in the Fig.7.

$$\gamma = \begin{cases} 1 & \text{When } \sigma_R < -\delta \text{ or } (\dot{\sigma}_R > 0 \text{ and } |\sigma_R| < \delta) \\ 0 & \text{When } \sigma_R > +\delta \text{ or } (\dot{\sigma}_R < 0 \text{ and } |\sigma_R| < \delta) \end{cases} \tag{33}$$

It can be seen from Fig.7 that the σ_R must increase from –δ to +δ during the Δt_1 ($\dot{\sigma}_R > 0$), while the σ_R must decrease from +δ to -δ during the Δt_2 ($\dot{\sigma}_R < 0$). Assuming that state trajectory remains the same near σ_R=0, the formula (34) for switching frequency can be deduced from Fig.7.

$$f_s = 1 \Big/ (\Delta t_1 + \Delta t_2) \tag{34}$$

Where, Δt_1 corresponds to the switching state γ=1, and Δt_2 to γ=0. And Δt_1 and Δt_2 can be solved by (35) and (36) respectively.

$$\Delta t_1 = 2\delta \Big/ \left(S_1 \cdot \frac{i_g^* + i_{dc1}^* - i_{dc1}}{C_2} + S_2 \cdot \frac{v_{C2} - v_{C2}^* + (1+N) \cdot V_{in}}{L_1 \cdot (1+N)} \right) \tag{35}$$

$$\Delta t_2 = -2\delta \Big/ \left(S_1 \cdot \frac{i_g^* + i_{dc1}^*}{C_2} + S_2 \cdot \frac{V_{in} - v_{C2}^*}{L_1 \cdot (1+N)} \right) \tag{36}$$

Substituting (35) and (36) into (34), the maximum switching frequency can be gotten as (37) at the positive peak value of v_{C2}, if assuming i_g^*=0 and the corresponding i_{dc1}^*=0 in the state of light load.

$$f_{smax} = \frac{S_2 \cdot V_{in}}{L_1 \cdot 2\delta} \cdot \frac{v_{C2}^* - V_{in}}{v_{C2}^* + N \cdot V_{in}} \tag{37}$$

The duty cycle ratio is defined as follows:

$$d_R(t) = \frac{\Delta t_1}{\Delta t_1 + \Delta t_2} \tag{38}$$

Substituting (34) and (35) into (38), the steady switching frequency can be gotten as (39), depending on the steady operation point such as duty cycle, control parameters and the value of grid current.

$$f_{SR}(t) = \left[d_R(t) / (2\delta) \right] \cdot \left[S_2 \cdot V_{in} / L_1 + S_1 \cdot i_g^*(t) / C_2 \right] \tag{39}$$

When i_g reaches negative peak value, the variation of i_{dc1} and $v_{C2}$is the largest, at this time, the duty cycle is the largest and the switching frequency the highest. As a consequence, L_1 and C_2 can be designed as (40) in order to ensure that all the magnetic components are unsaturated within the scope of the switching frequency.

$$L_1(t) \geq \frac{V_{in} \cdot d_{R\max}}{\Delta I_{dc1\max} \cdot f_{SR\min}} \quad and \quad C_2 \geq \frac{I_g^* \cdot d_{R\max}}{\Delta V_{C2\max} \cdot f_{SR\min}} \tag{40}$$

B. The Implementation of Left-Side SMC

Since the left side is the third order system, the sliding mode surface σ_L can be chosen by (41).

$$\sigma_L = S_3 \cdot \varepsilon i_g + S_4 \cdot \varepsilon v_{C1} + S_5 \cdot \varepsilon i_{dc2} \tag{41}$$

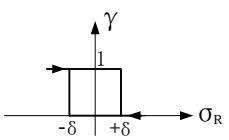

Fig.6. Switching function γ.

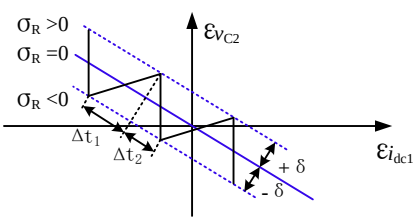

Fig.7. The waveform of σ_R.

Let S_L=[S_3, S_4, S_5]^T, the expression (41) can be written by (42).

$$\sigma_L = S_L^T y \tag{42}$$

Since the error variables are defined by (19), whenever the representative point lies below the switching line σ_L, the energy in the elements C_1 and L_3 is little, and thus λ is set to 1, conversely, the energy is surplus when the representative point lies above the switching line σ_L, and λ are set to 0. So the expression (43) can be gotten.

$$\lambda = \begin{cases} 1 \text{ When } \sigma_L < 0 \\ 0 \text{ When } \sigma_L > 0 \end{cases} \quad (43)$$

Due to that the error variables is very small and approaches to zero by comparing with the reference values, so the existing condition (25) for sliding mode surface on the left side can be written by (44) and (45).

$$\dot{\sigma}_L = S^T D^{'} < 0, \ \ \sigma_L > 0 \quad (44)$$

$$\dot{\sigma}_L = S_L{}^T B^{'} + S_L{}^T D^{'} > 0, \ \ \sigma_L < 0 \quad (45)$$

Substituting the matrix $B^{'}$ and $D^{'}$ into (44) and (45) respectively, the expression (46) and (47) can be gotten.

$$S_3 \frac{v_{C1}{}^* - v_{C2}{}^* - V_g}{L_{ac}} + S_4 \frac{i_{dc2}{}^* - i_g{}^*}{C_1} + S_5 \frac{V_{in} - v_{C1}{}^*}{L_3 \cdot (1+N)} < 0 \quad (46)$$

$$S_3 \frac{v_{C1}{}^* - v_{C2}{}^* - V_g}{L_{ac}} + S_4 \frac{i_{dc2}{}^* - i_{dc2} - i_g{}^*}{C_1} + S_5 \frac{V_{in}(1+N) + v_{C1} - v_{C1}{}^*}{L_3 \cdot (1+N)} > 0 \quad (47)$$

If the expression (46) and (47) are established, the existing condition for the sliding mode will be met. And the sufficient condition for the existence of the sliding mode surface defined by (41) is that S_3, S_4 and S_5 choose nonnegative values.

Just like the right side, the hysteresis comparison control is employed to avoid excessive switching frequency. Here, assuming that the hysteresis width is 2ζ, the phase plane trajectory will oscillate on both sides of the sliding mode surface(σ_L=0)

Defining the on time of switch T_3 for Δt_1 that corresponds to the switching state λ=1, and the off time for Δt_2 that corresponds to the switching state λ=0, Δt_1andΔt_2can be solved by (48) and (49) respectively.

$$\Delta t_1 = \frac{2\xi}{\left(S_3 \frac{v_{C1}{}^* - v_{C2}{}^* - V_g}{L_{ac}} + S_4 \cdot \frac{i_{dc2}{}^* - i_{dc2} - i_g{}^*}{C_1} + S_5 \cdot \frac{V_{in}(1+N) + v_{C1} - v_{C1}{}^*}{L_3 \cdot (1+N)} \right)} \quad (48)$$

$$\Delta t_2 = \frac{-2\xi}{\left(S_3 \frac{v_{C1}{}^* - v_{C2}{}^* - V_g}{L_{ac}} + S_4 \frac{i_{dc2}{}^* - i_g{}^*}{C_1} + S_5 \frac{V_{in} - v_{C1}{}^*}{L_3 \cdot (1+N)} \right)} \quad (49)$$

Just the same with the right-side converter, the maximum switching frequency happens at the light load. Assuming that i_g*=0 and the corresponding i_{dc2}*=0, and noticing that the coefficient of terms S_3 is zero and the terms of S_4 and S_5 like (35) and (36), the expression (50) can be gotten.

$$f_{smax} = \frac{S_4 \cdot V_{in}}{L_3 \cdot 2\zeta} \cdot \frac{v_{C1}{}^* - V_{in}}{v_{C1}{}^* + N \cdot V_{in}} \quad (50)$$

It can be seen that the last two terms are the same with the right side in the existing condition (46) and (47) for sliding mode surface of the left-side converter, i.e., S_4=S_1, S_5=S_2. So only the value of S_3 needs to be confirmed. Since the CIDBI is used as grid connected power generation, $v_{C1}{}^* - v_{C2}{}^* - V_g > 0$ in (46) must be established and this difference value should equal to v_{Lac} of L_{ac}, thus S_3>0 ; as a consequence, the upper limit of S_3 can be solved by (46) under the condition of the maximum of $\left| v_{Lac} \right|$.

The steady state switching frequency can be solved by (51) only if Δt_1+Δt_2 iscalculated during the period of hysteresis which is like the right side.

$$f_{SL}(t) = \left[d_L(t) / (2\zeta) \right] \cdot \left[S_5 \cdot V_{in} / L_3 - S_4 \cdot i_g{}^*(t) / C_1 \right] \quad (51)$$

When i_g reaches the positive peak value, the variation of i_{dc2} and v_{C1} is the largest, and hence, the values of L_3 and C_1 can be chosen by (52).

$$L_3(t) \geq \frac{V_{in} \cdot d_{L\max}}{\Delta I_{dc2\max} \cdot f_{SL\min}} \ \ and \ \ C_1 \geq \frac{I_g{}^* \cdot d_{L\max}}{\Delta V_{C2\max} \cdot f_{SL\min}} \quad (52)$$

The application of such high-pass filters is preferred to the use of a calculated reference for the secondary variables. Since the controller seeks to nullify the weighted *sum* of errors, and not an error in particular. Thus, if one of those references is determined incorrectly, this would result in tracking imperfections in the output variables. This technique is well suited to dc-dc converter. In the present application, the low-frequency ac evolutions (up to doubled mains frequency) can be considered as quasi static state, therefore the derivative of these variables can be thought of as zero. In the feedback, the low-frequency components are filtered by high-pass filter, it can be considered that the low-frequency components have tracked the reference value in the steady state, and only high-frequency components including high-frequency components and even the spike need to be regulated.

So it is feasible to collect indirect variables with high-pass filter. Of course, the introduction of the high-pass filter will increase the order of the system. Generally speaking, during transients, the response becomes more oscillatory than it would be using defined references for the secondary variables. It is desirable to have fast filters with high cutoff frequency, in order not to alter greatly the dynamics of the circuit. But on the other hand they must present some sensitivity to the resonant frequency of L_1 and C_1 or L_2 and C_2, remembering that the resonant frequency in a switched circuit depends also on the duty cycle. One must observe that, for safety concerns, a current limitation must be implemented for the dc inductors, because the system with filters is not sensitive to the value of the current when the switch is on for a long period of time(this is especially true during start-up).

Also the selection of L_{ac} is conditioned by the high-pass filters, especially by the filter forv_{C1}, which must be sensitive to the resonant frequency between L_{ac}, and the series

association of C_1 and C_2.

IV. Design Example and Experimental Results

In order to verify the correctness of the above theoretical analysis, a two-channel experimental prototype is built as shown in Fig.8. and each channel is connected to a photovoltaic module. Here, the performance parameters of only one channel are given here. The input dc source is PV array whose open voltage is 44V and the maximum power point (MPP) voltage is 35V. The prototype specifications are listed in the Tab.I.

In order to regulate grid current i_g linearly with the duty cycle ranging from 0.3 to 0.75, the dc bias voltage V_{dc} choose 280V, and the turn ratio of the coupled inductor is 4. Assuming that the grid current is 1.43Arms at MPP, the reference current and voltage are as follows.

$$\begin{cases} i_g^*(t) = 1.43\sin(\omega t) \\ v_{C2}^*(t) = 162.6\sin(\omega t + \pi) + 280 \end{cases} \tag{59}$$

It is clear that V_{C2max}=442.6V.

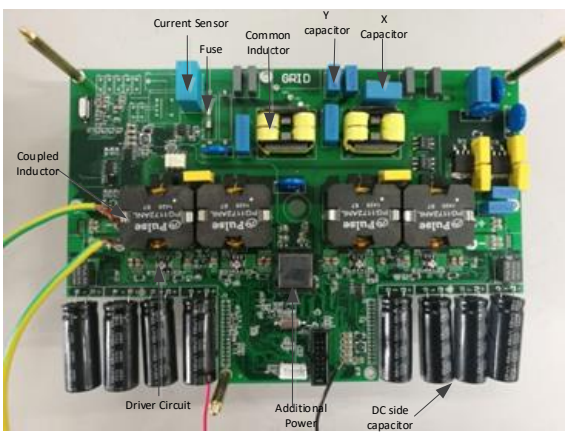

Fig.8. Experimental prototype of photovoltaic grid-connected micro-inverters based on CIDBI.

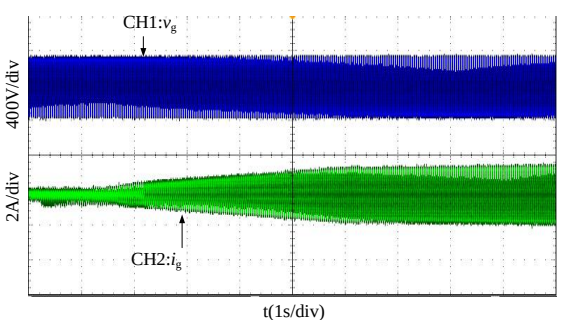

Fig.10. Start-up generation waveform of micro inverter.

TABLE I

THE PROTOTYPE SPECIFICATIONS

Output power:Po	480W
Grid maximum voltage: v_g	230Vrms
MPP voltage: V_{in}	35V
Grid frequency: f_0	50Hz
Maximum switching frequency:f_{smax}	130kHz

DC capacitors C_1 choose 6×2200μF, T_1 and T_3 choose IPB072N15N3G from Infineon (150V/93A @100°C), Rdson=7.2mΩ; T_2 and T_4 choose SPB17N80C3 from Infineon (800V/17A @100°). Main experimental waveforms are given in the Fig.9, here, v_g is utility grid voltage, i_g is grid connected current, and v_{pv} is the PV voltage. The Fig.9(a) shows the steady operation waveforms with PI controller in reference [1] and Fig.9(b) presents the waveforms based on SMC in this paper, and the grid connected current waveforms i_g(CH3) in the Fig.9(b) is clearly much better than that in the Fig.9(a). When the output power reaches to 221W, the efficiency of CIDBI is greater than 95.8%, the total harmonic distortion of i_g is equal to 1.52%, and the power factor is not less than 0.99. It is clear that the presented sliding mode controller can be applied to CIDBI and transfer energy from dc side to mains grid with high quality.

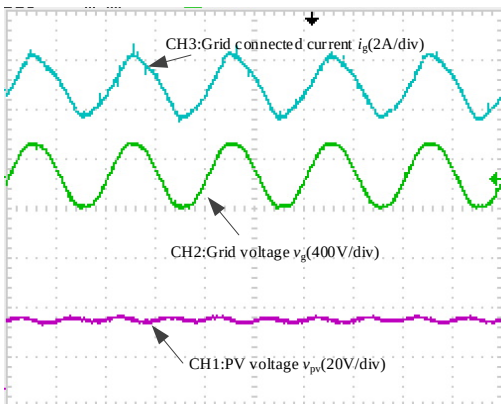

(a) With PI controller in reference [1]

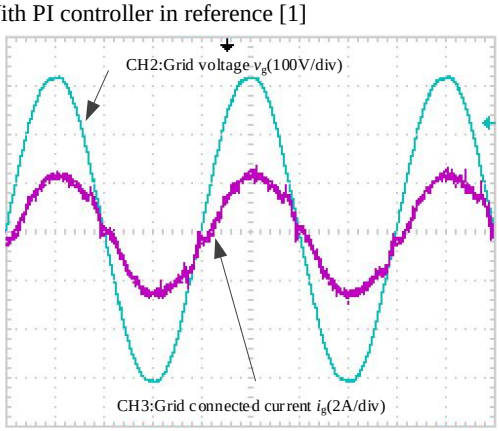

(b) With SMC in this paper

Fig.9. The main steady operation waveforms in the grid-connected generation.

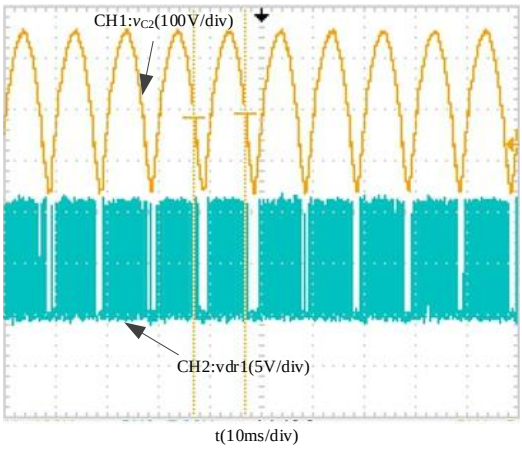

Fig.11. Driving waveform of T1 & voltage on C_2 in right-side circuit.

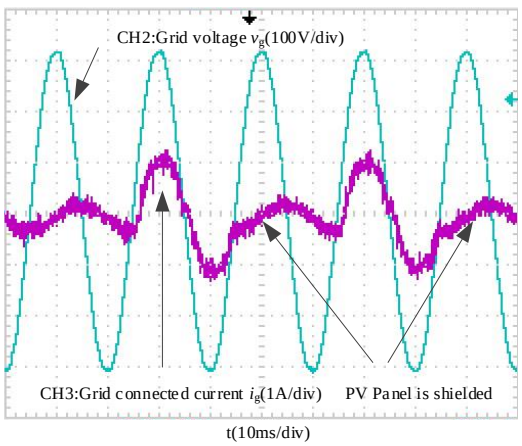

Fig.12. Occlusion experiment of photovoltaic module.

Fig.10 shows the waveforms of grid voltage and grid-connected current when the prototype starts. As can be seen from the figure, when the prototype starts to grid-connected power generation, the current i_g begins to increase gradually. After a period of time, the current reaches its maximum value and constant. Channel 1 of Fig.11 shows the voltage waveform on capacitor C_2 in the right circuit of CIDBI, and channel 2 is the driving waveform of switch T_1. Channel 3 of Fig.12 shows the grid-connected current waveform (i_g) when the photovoltaic panel is shielded or not, and channel 2 of Fig.12 is grid voltage. From the above experimental waveforms, using the two sliding mode controllers proposed in this paper can not only obtain the stability of micro-inverters based on CIDBI architecture, but also obtain fast dynamic response speed.

V. Conclusions

The CIDBI can be used to generate an ac output voltage larger than the dc input one and transfer the energy from PV array or dc energy storage device to the grid with only one power processing stage. Aiming at the problem that it is difficult to design parameters of traditional regulators for high-order systems of CIDBI circuits, the different sliding-mode controllers are proposed respectively on the right-side converter and the left-side one with different switching scheme in this paper, and the SMCs can track the time-varying reference functions very well. These functions are only defined for the two output variables; other secondary signals are obtained after high-pass filtering. The use of such SMCs can achieve overall performance of the system remarkably.

Acknowledgments

This paper was supported in part by the National Natural Science Foundation of China under Grant 61873346, in part by the Science and Technology Cooperation Fund of Yangzhou City Hall project under Grant YZ2018136, in part by the Intelligent Energy Internet Research Institute Joint Fund of State Grid Yangzhou Power Supply Company and Yangzhou University under Grant SGTYHT/17-JS-202, and in part by the Open Project Fund of Yangzhou University Jiangdu Institute of High-end Equipment Engineering Technology under Grant YDJD201902.

References

[1] Yu Fang and Xudong Ma, "A novel PV micro inverter with coupled inductors and double-boost topology," *IEEE Transactions on Power Electronics*, Vol.25, No. 12, pp. 3139-3147, 2010.

[2] Kaihui Zhao; Tonghuan Yin; Changfan Zhang; Jing He;Xiangfei Li; Yue Chen; Ruirui Zhou; Aojie Leng, "Robust model-free nonsingular terminal sliding mode control for PMSM demagnetization fault," *IEEE Acce*ss, pp.15737-15748, 2019.

[3] Yang Yueneng; Yan Ye, "Back stepping sliding mode control for uncertain strict-feedback nonlinear systems using neural-network-based adaptive gain scheduling," *Journal of Systems Engineering and Electronics*, Vol. 29, No. 3, pp.580-586, 2018.

[4] Aysar Musa ; Lorenzo R.Sabug; Antonello Monti. "Robust predictive sliding mode control for multiterminal HVDC grids," *IEEE Transactions on Power Delivery*, Vol. 33, No. 4, pp.1545-1555, 2018.

[5] Mohammad B. Delghavi ; Amirnaser Yazdani, "Sliding-mode control of AC voltages and currents of dispatchable distributed rnergy resources in master-slave-organized inverter-based microgrids," *IEEE Transactions on Smart Grid*, Vol. 10, No. 1, 980-991, 2019.

[6] Woonki Na ; Kohl, R. ; Weider Chung, "Sliding mode control of a power factor corrected converter for Plug-In Hybrid Electric Vehicles," *38th Annual Conference on IEEE Industrial Electronics Society (IECON)*, pp. 763-767, 2012.

[7] Rong-Jong Wai ; Li-Zon Shin, "Total sliding-mode voltage tracking control for DC-DC boost converter," *6th IEEE Conference on Industrial Electronics and Applications (ICIEA)*, pp.2676-2681, 2011.

[8] Rong-Jong Wai ; Li-Chung Shih, "Design of voltage tracking control for DC–DC boost converter via total sliding-mode technique," *IEEE Transactions on Industrial Electronics*, Vol. 58, No. 6, pp.2502-2511, 2010.

[9] Salimi, M. ; Soltani, J. ; Zakipour, A. ; Hajbani, V., "Sliding mode control of the DC-DC flyback converter with zero

steady-state error," *4th Power Electronics, Drive Systems and Technologies Conference (PEDSTC)*, pp.158-163. 2013.

[10] Michele Cucuzzella ; Gian Paolo Incremona ; Antonella Ferrara, "Decentralized sliding mode control of islanded AC microgrids with arbitrary topology," *IEEE Transactions on Industrial Electronics*, Vol.64, No.8, pp.6706-6713, 2017.

[11] Rui Ling; Yan Dong; Meirong Wu; Yi Chai, "Decentralized sliding mode control of WG/PV/FC micro grids under unbalanced and nonlinear load conditions for on- and off-grid modes," *IEEE Systems Journal*, Vol. 12, No. 4, pp.3108-3119, 2018.

[12] Hao Ma ;Qinwei Liu ; Jin Guo, "A sliding-mode control scheme for LLC resonant DC/DC converter with fast transient response," *38th Annual Conference on IEEE Industrial Electronics Society(IECON)*, pp.162-167, 2012.

[13] Muhammad Ali Masood Cheema ; John Edward Fletcher ; Mohammad Farshadnia ;Muhammad Faz Rahman, "Sliding mode based combined speed and direct thrust force control of linear permanent magnet synchronous motors with first-order plus integral sliding condition," *IEEE Transactions on Power Electronics*, Vol.34, No.3, 2526-2538, 2019

[14] Monteiro, J. ; Silva, J.F. ; Pinto, S.F. ; Palma, J., "Linear and sliding-mode control design for matrix converter-based unified power flow controllers," *IEEE Transactions on Power Electronics*, Vol.29, No. 7, pp. 3357-3367, 2014.

[15] Labbe, B. ; Allard, B. ; Xuefang Lin-Shi ; Chesneau, D., "An integrated sliding-mode buck converter with switching frequency control for battery-powered applications," *IEEE Transactions on Power Electronics*, Vol.28, No. 9, pp.4318-4326, 2013.

[16] Guanghui Sun ; Zhiqiang Ma ; Jinyong Yu., "Discrete-time fractional order terminal sliding mode tracking control for linear motor," *IEEE Transactions on Industrial Electronics*, Vol. 65, No. 4, pp.3386-3394, 2018.

[17] Lijun Zheng ; Fayang Jiang ; Jiancheng Song ; Yunguang Gao ; Muqin Tian, "A discrete-time repetitive sliding mode control for voltage source inverters," *IEEE Journal of Emerging and Selected Topics in Power Electronics*, Vol. 6, No. 3, pp.1553-1566, 2018.

[18] Haroun,R.;Cid-Pastor,A.;El Aroudi,A.; Martinez-Salamero, L.,"Synthesis of canonical elements for power processing in DC distribution systems using cascaded converters and sliding-mode control," *IEEE Transactions on Power Electronics*, Vol.29, No.3, pp.1366-1381, 2014.

[19] Singh, P.K. ; Hote, Y.V. ; Garg, M.M., "Comments on PI and sliding mode control of a cuk converter," *IEEE Transactions on Power Electronics*, Vol.29, No.3, pp.1551-1552, 2014.

[20] Youdong Lv Haisheng Yu; Xudong Liu, "Switching Control of Sliding Mode and passive control for DC-Link voltage of isolated shoot-through Z-source inverter," *Chinese Automation Congress (CAC)*, pp.2687-2692, 2018.

[21] Gian Paolo Incremona ; Matteo Rubagotti ; Antonella Ferrara, "Sliding mode control of constrained nonlinear systems," *IEEE Transactions on Automatic Contro*l,Vol. 62, No.6, pp.2965-2972, 2017.

[22] Song Jian ; Liu Zhitao ; Su Hongye, "A second-order sliding mode control design for bidirectional DCDC converter," *36th Chinese Control Conference (CCC)*, pp.9181-9186, 2017.

[23] Hong Liu ; Dianwei Qian, "Sliding-mode-based disturbance rejection control of nonlinear power systems with renewable sources," *International Conference on Advanced Mechatronic Systems (ICAMechS)*, pp. 238-243, 2015.

[24] Xiangcai Meng ; Haisheng Yu ; Xudong Liu, "Adaptive backstepping speed control and sliding mode current regulation of permanent magnet synchronous motor," Chinese Control And Decision Conference (CCDC), pp.4025-4029, 2018.

[25] Hai-Peng Ren ; Ren Zhou, "Fuzzy sliding mode tracking control for DC motor servo system without uncertainty information," *12th IEEE Conference on Industrial Electronics and Applications (ICIEA)*, pp.1511-1515, 2017.

[26] Y Gian Paolo Incremona ; Matteo Rubagotti ; Antonella Ferrara, "Sliding mode control of constrained nonlinear systems," *IEEE Transactions on Automatic Control*, Vol.62, No.6, pp.2965-2972, 2017.

[27] Sanjeev Kumar Pandey ; Sanjaykumar Limaji Patil ; Shrivijay B. Phadke, "Comment on PWM-based adaptive sliding-mode control for Boost DC–DC converters, " *IEEE Transactions on Industrial Electronics,* Vol.65, No.6, pp.5078-5080, 2018.